Reinjection probability density for type-III intermittency with noise and lower boundary of reinjection

Sergio Elaskar
Professor,
IDIT and Aeronautical Department
National University Cordoba - CONICET
Cordoba, Argentina
Email: selaskar@unc.edu.ar

Ezequiel del Rio
Professor,
E.T.S.I. Aeronicos
Polytechnic University Madrid
Madrid, Spain

Andrea Costa
Professor,
IATE and Aeronautical Department
National University Cordoba - CONICET
Cordoba, Argentina

ABSTRACT

In this paper we extend a methodology developed recently to study type-III intermittency considering different values of the noise intensity and the lower boundary of reinjection (LBR). We obtain accurate analytic expressions for the reinjection probability density (RPD). The proposed RPD has a piecewise definition depending on the nonlinear behavior, the LBR value and the noise intensity. The new RPD is a sum of exponential functions with exponent $\alpha+2$, where α is the exponent of the noiseless RPD. The theoretical results are verified with numerical simulations.

1 Introduction

One of the routes to chaos is produced by intermittency, where the dynamic system has transitions between regular (or laminar) phases and chaotic bursts (or non regular phases). The laminar phases are regions of pseudo-equilibrium and/or pseudo-periodic solutions and the burst ones are regions where the evolution is chaotic. The concept of intermittency was introduced by Pomeau and Manneville [1, 2]. Traditionally, intermittency is classified into three different types called I, II and III [3, 4] according to the Floquet multipliers of the system or to the eigenvalues of the local Poincaré map. More recent studies have extended the classification to other types of intermittencies such as type V, X, on-off, eyelet, ring and in-out [5–10].

Considering type I, II and III intermittency phenomena, when a control parameter exceeds a threshold value, a bifurcation leads to a change of the system behavior towards a chaotic motion. In all cases, a fixed point of the local Poincaré map becomes unstable or even vanishes for some values of the control parameter ε. Intermittency has been observed in several physical topics such as the Lorenz system, Rayleigh-Bénard convection, forced nonlinear oscillators, plasma physics, electronic circuits, turbulent flows [11–16]. Also, intermittency has been used to describe the behavior of economy and medicine systems [17–19]. The accurate description of intermittency helps to improve the knowledge about these phenomena. On the other hand, the proper characterization of the RDP function is important for a correct description of intermittency.

Type-III intermittency occurs in a subcritical period-doubling bifurcation in which an unstable period-2 orbit meets and destabilizes a stable period-1 orbit; this type of intermittency is characterized by the gradual increasing during the laminar phase of a period-2 component in the motion [20]. A one dimensional map $f(x)$ that displays a subcritical period-doubling bifurcation has a positive Schwartzian derivative: $Sf(x) = f'''(x)/f'(x) - 1.5\,(f''(x)/f'(x))^2 > 0$.

Intermittency can be studied using Poincaré maps [3, 4], which have two main chaotic intermittency characteristics: 1) a specific local map and 2) a reinjection mechanism. The local Poincaré map for type-III intermittency is given by: $x_{n+1} = -(1+\varepsilon)x_n - a\,x_n^3$, where the control parameter ε and the coefficient a are larger than zero [20, 21]. The reinjection mechanism maps the system back into the local regular or laminar zone from the chaotic one. This mechanism is described

by means of a probability function called reinjection probability density (RPD) which gives the probability that trajectories are reinjected into the laminar zone, close to the unstable fixed point. This function depends on the nonlinear dynamics of the system itself and can lead to a broad range of different behaviors. Therefore, it is not an easy task to obtain an analytical expression for the RPD; only in few cases this is possible. A direct experimental or numerical evaluation of the RPD function is also not a simple task due to the huge amount of data needed to deal with. Moreover, the statistical fluctuations induced in the numerical computations and the experimental measurements are difficult to estimate.

As noise is always present in nature [22], it is important to describe how it affects the intermittent RPD. The noise effects on the intermittency phenomenon was studied using a renormalization group analysis and the Fokker-Plank equation [23–25]. Note that all the mentioned references analyze the effects of noise on the laminar zone; however, it has been recently shown that noise strongly influences the RPD function [26,27]. Moreover, as there is experimental evidence of the lower boundary of reinjection (LBR) for type III intermittency [11] we decided to focus in the analysis of phenomena with type-III intermittency where LBR and noise are present.

The RPD function allows to determine the statistical properties of the intermittency process like the average laminar length -the average time that trajectories spend close to the vanished or unstable limit cycle-, and the characteristic equation -the scaling relation of the average laminar length. The characteristic equation gives the relation between the average laminar length, $\bar{l}$ and the control parameter ε: $\bar{l} \sim \varepsilon^{-\beta}$, where β is the characteristic exponent of the scaling relation and depends on of reinjection probability distribution. This characteristic relation allows to estimate the duration of the laminar phases -the time interval between chaotic phases. They depend on the RPD, which depends on the global maps behavior. Therefore, the accurate evaluation of the RPD function is extremely important to describe the chaotic intermittency. Several approaches were used to obtain the intermittent RPD function. The usual assumption is to consider a uniform reinjection using a constant RPD function [3,4]. Other implemented approaches built the RPD using peculiar features of the nonlinear processes. Nevertheless, these RPD functions cannot be successfully applied to other nonlinear systems. Two examples are given in [25,28]: 1) for type-III intermittency in an electronic circuit the RPD was considered proportional to $1/\sqrt{x-x_s}$ in [25], and 2) to investigate the effect of noise in type-I intermittency, it is assumed that the reinjection is localized in a fixed point [28]. There was not an efficient method to obtain the RPD function until a general technique, called here M methodology, which includes the uniform reinjection as a particular case, was introduced in the last years [21,26,29–34]. In this paper this general methodology is used to describe the reinjection processes for type-III intermittency considering noise effects, and to extend the effects of noise to cases not previously considered as lower boundaries of reinjection different from zero (LBR $\neq 0$). Several new theoretical noisy RPD functions defined as the addition of exponential functions are obtained. The new noisy RPD functions are compared with numerical results showing a very good agreement for two maps with different non-linear behaviors.

2 Type-III Intermittency

We analyze two one dimensional maps with type-III intermittency. We select these maps because they were studied using the M methodology in preceding papers [21, 31]. However, these papers do not analyze the effects of noise and LBR on the RPD function. Both maps have a fixed point in $x = 0$, and they are symmetric around this point. The first map was presented in [21], and can be written as:

$$x_{n+1} = F(x_n) = -(1+\varepsilon)x_n - ax_n^3 + bx_n^6 sin(x_n) \tag{1}$$

where ε is the control parameter. The map has a fix point $x_0 = 0$ at the origin, which is stable for $-2 < \varepsilon < 0$. When $\varepsilon > 0$, the fix point becomes unstable and type-III intermittency arises. The reinjection mechanism depends on the map extreme values, x_m, satisfying $dF(x_m)/dx = 0$ (see Figure 1). In particular, this odd map has two extreme points. The iteration procedure, which is governed by the parameters ε, a and the cubic exponent, leads to increasing values of x_n generated from an initial one, close to the origin. For large enough values of n, the influence of the RHS third terms in Eq. (1) increases as x_n approaches to an extreme point x_m, rendering the reinjection into the laminar zone.

The second map was given in [20]:

$$x_{n+1} = F(x_n) = -((1+\varepsilon)x_n + x_n^3)e^{-bx_n^2} \tag{2}$$

This map has a single fix point at $x_0 = 0$ with a slope $dF(x_0)/dx = -(1+\varepsilon)$, being stable for $-2 < \varepsilon < 0$. There is a subcritical period-doubling bifurcation at $\varepsilon = 0$ for $b < 1$. The reinjection mechanism is governed by the factor $e^{-bx_n^2}$: when the amplitude x_n is large enough, this factor becomes small and the iteration $n+1$ falls close the unstable fix point (see Figure 1).

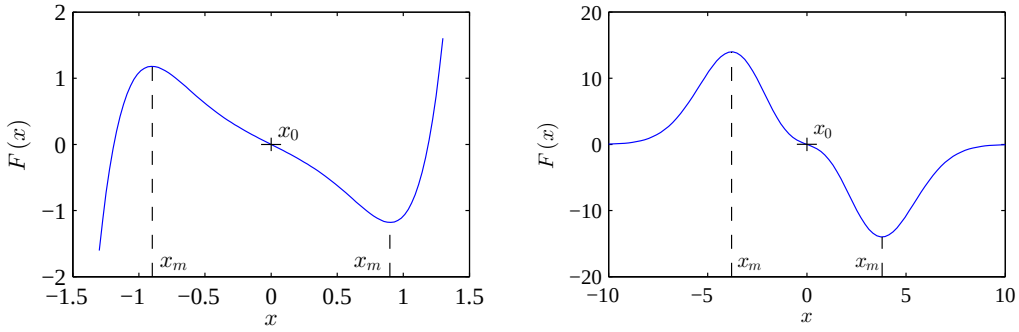

Fig. 1. Left: Map (1). The parameters are: $\varepsilon = 0.01$, $a = 1,0$ and $b = 1.1$. Right: Map (2). The parameters are: $\varepsilon = 0.1$ and $b = 0.1$.

Both maps have x_m points with $dF(x_m)/dx = 0$ (local maximum or local minimum). These points have a strong influence on the reinjection processes, but the reinjection mechanism is different for each map because the derivative $dF(x_n)/dx$, where x_{n+1} is a reinjected point inside the laminar interval, are different. Therefore, the implementation of these two maps permits to analyze different non-linear behaviors, i.e., different reinjection processes. We highlight the points close to x_m need two iterations to be reinjected.

3 Evaluation of the RPD function. The M methodology.

The description of the theoretical framework that accounts for a wide class of maps and dynamical systems exhibiting intermittency, called M methodology, is briefly presented. Consider a general one-dimensional map: $x_{n+1} = F(x_n)$. The noiseless RPD function, denoted here by $\phi(x)$, determines the probability that trajectories are reinjected into a point x inside the laminar interval. The RPD specifies the statistical behavior of the reinjection trajectories, which depends on the specific form of $F(x)$ [3,4].

In the methodology developed to deal with intermittency the RPD function is not directly obtained from the numerical or experimental data. A new function, $M(x)$, is calculated [21, 26, 29–32]:

$$M(x) = \begin{cases} \dfrac{\int_{x_s}^{x} \tau\phi(\tau)\,d\tau}{\int_{x_s}^{x} \phi(\tau)\,d\tau}, & \text{if } \int_{x_s}^{x} \phi(\tau)\,d\tau \neq 0, \\ 0, & \text{otherwise,} \end{cases} \tag{3}$$

where τ represents the reinjected points around the unstable fixed point, and x_s is the closest reinjection point to the unstable fixed point, i.e., the lower boundary of reinjection point. To calculate $M(x)$, the symmetry reinjection process around the fixed point is considered; only $x \geq 0$ are used.

$M(x)$ is an auxiliary function used to evaluate the RPD, it is a quotient between two integrals which softens the fluctuations of the experimental or numerical data used to construct it [21, 26, 29–34]. On the other hand, $M(x)$ corresponds to the average over the reinjection points in the laminar interval, hence its numerical estimation is more robust than the direct evaluation of the function $\phi(x)$. In addition, the calculation of $M(x)$ from the data series is very simple: $M(x) \cong \frac{1}{N}\sum_{j=1}^{N} x_j$, where the data set (reinjection points) $\{x_j\}_{j=1}^{N}$ must be sorted from the lowest to the highest, i.e. $x_j \leq x_{j+1}$.

In previous papers, we found that $M(x)$ satisfies a linear approximation for a wide class of maps exhibiting type I, II and III intermittencies without noise [21, 26, 29, 30, 32]:

$$M(x) = \begin{cases} m(x - x_s) + x_s, & \text{if } x_s \leq x \leq c, \\ 0, & \text{otherwise,} \end{cases} \tag{4}$$

where the slope $m \in (0,1)$ is a free parameter -determined for the non-linear map- that governs the reinjection process. Introducing Eq. (7) in Eq. (6) the corresponding RPD function results [21, 29, 30]:

$$\phi(x) = \lambda(x - x_s)^{\alpha}, \quad \text{with} \quad \alpha = \frac{2m-1}{1-m}, \tag{5}$$

where λ is a normalization parameter. The usually considered uniform RPD is recovered for $m = 1/2$ ($\alpha = 0$), i.e., uniform

reinjection is obtained as a particular case of the new theoretical formulation. Note that $\phi(x)$ can depart from a uniform reinjection, e.g., $\lim_{x\to 0}\phi(x)$ is infinity when $0 < m < 1/2$ ($\alpha < 0$) and zero, when $1/2 < m < 1$ ($\alpha > 0$).

The $M(x)$ function is only determined by the parameter m, and it is easier to obtain among a huge amount of data than the complete RPD function. Also $M(x)$ satisfies $M(x_s) = x_s$; then, it allows to evaluate the LBR. For both maps, $M(x)$ without noise was numerically evaluated obtaining a linear form $M(x) = m(x - x_s) + x_s$ for different values of b, a and ε [21]. Hence, the RPD function can be expressed by Eq. (8) with $\lambda = 0.5(\alpha+1)/(c-x_s)^{\alpha+1}$.

As the slope m determines the value of the exponent α in the RPD function (see Eq. (8)), it rules the reinjection mechanism and has direct influence in the probability density of the laminar length, in the average laminar length and in the characteristic relation. The probability density of the laminar lengths, $\phi_l(l)$, is a global property and is related to the reinjection probability density function, $\phi(l,c)$, by the expression [21, 29]: $\phi_l(l,c) = 2\lambda\,[x(l,c) - x_s]^{\alpha}\,[\varepsilon x(l,c) + a x(l,c)^p]$, where l is the laminar length.

For inttermitency without noise, the M function is determined by the nonlinear map; each map produces a different M function, defined by the parameters m and x_s. Then, the M function stores the nonlinear information of the map [35, 36].

4 Noise influence for LBR = 0

In this section the influence of noise on the statistical properties of type-III intermittency is analyzed [26]. Noise, present in all natural dynamical system, will affect the RPD function. It is usually assumed that the noise strength σ is much smaller than the control parameter ε. Here, we consider a general procedure where this hypothesis is avoided by transforming (1) and (2) into noisy maps:

$$x_{n+1} = F(x_n) = -(1+\varepsilon)x_n - a x_n^3 + d x_n^3 sin(x_n) + \sigma\xi_n \tag{6}$$

$$x_{n+1} = F(x_n) = -((1+\varepsilon)x_n + x_n^3)e^{(-b x_n^2)} + \sigma\xi_n \tag{7}$$

where ξ_n is a uniform distributed noise verifying that $\langle \xi_m, \xi_n \rangle = \delta(m-n)$ and $\langle \xi_n \rangle = 0$, with noise strength σ. Note that if $\sigma = 0$, the previous maps (1) and (2) are recovered.

The reinjection processes in both maps (1) and (2) are different that those for type-II intermittency described in [27]. For type-III intermittency, a point (a trajectory) laying very close to the extreme points (maximum or minimum) will need two iterations to be reinjected into the laminar zone. On the other hand, for type-II intermittency only one iteration was necessary [27]. Through these iterations, type-III intermittency trajectories are stretching or contracting by the derivative $K = dF(x_n)/dx$, where $x_{n+1} = F(x_n)$ is a reinjected point into the laminar zone. The map (1) strengthens the trajectories, however the map (2) can contract them. The slope K varies as x_n changes, however in most maps, K can be approximated by a constant because the laminar interval is small around the unstable fixed point. Accordingly, K corresponds to the mean slope of the curve in the interval I, where I is the interval mapped backward of the laminar region.

Figure 2 shows the numerical results for the noisy $M(x)$ considering Eq. (9) with $\varepsilon = 0.01$, $a = 1.1$, $b = 1.35$, $c = 0.6$ and $\sigma = 0.02$. To compare results we have considered, following the papers [21, 26], that the laminar interval length verifies $c = 0.6$. As for the noiseless case, the functions $M(x)$ smooths down the data. However, for the noisy tests, the function $M(x)$ has different behavior on each side of x_c. We call singular points to those points where the behavior of $M(x)$ changes, e.g., x_c. $M(x)$ can be approximated by a piecewise linear function with two slopes. The x_c value is approximately equal to the product between the noise intensity and the slope K, $x_c \cong K\sigma$. Note that $\sigma_r = K\sigma$ is the amplified noise intensity in the reinjected point. For the figure $K \cong 11$; therefore, $\sigma_r \cong 0.22$. For $x < x_c$ the slope of $M(x)$, m_l, approaches $1/2$, as expected for the uniform reinjection. For $x > x_c$, the slope of $M(x)$, m_r is similar to the noiseless slope. The total number of reinjected point used was 300000, and 53483 reinjected points were used to evaluate m_r (we calculate m_r using the points indicated by the darker (blue) line in Figure 2). This is a remarkable property of $M(x)$ because we can obtain the RPD function for the noiseless case by means of a noisy data analysis. Note that even when noise acts on the complete system, it does not modify the slope of $M(x)$ in the region $x > x_c$. Hence, on the right side of x_c, the RPD function is robust against noise without adjacent reinjection [26, 27]. However, in the region $x < x_c$ the noise modifies the RPD. When noise is considered and $x < x_c$, the RPD approaches the uniform reinjection case, at least locally around the unstable fix point $x_0 = 0$, due to the symmetry of the map around it. Therefore, point x_c is a boundary that separates two regions inside the laminar zone. One region is $[0, x_c]$ in which the noise governs the reinjection procces. The other region is $(x_c, c]$ in which the nonlinear map drives the intermittency reinjection.

Following reference [26] we obtained an analytical expression for the noisy reinjection probability density, called NRPD.

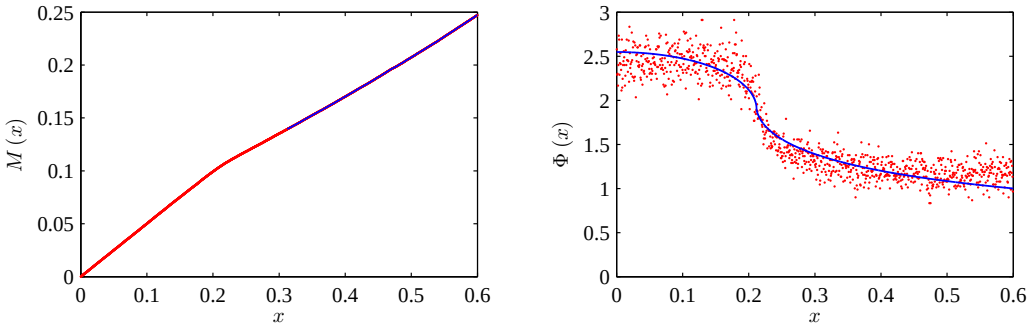

Fig. 2. Map (9). Left: $M(x)$ from the numerical simulations, the darker (blue) line indicates the data used to calculate the exponent α. Right: Theoretical and numerical RPD functions, the points corresponds to numerical data, the result of Eq. (13) is plotted as a solid line. Parameters: $\varepsilon = 0.0005$, $c = 0.6$, $a = 1.1$ and $b = 1.35$, $K = 10.5833$.

The noiseless density $\phi(x)$ transforms in a new density $\Phi(x)$ according to the convolution integral:

$$\Phi(x) = \int \phi(y) G(x-y, K\sigma)\, \mathrm{d}y \tag{8}$$

where $\Phi(x)$ is the NRPD and $G(x,\sigma)$ is the probability density of the noise term $\sigma\xi_n$. A random variable ξ in the interval $[-1,1]$ is used as a noise source, then its probability density $G(x,\sigma)$ results:

$$G(x,\sigma) = \frac{\Theta(x+K\sigma) - \Theta(x-K\sigma)}{2K\sigma} \tag{9}$$

where $\Theta(x)$ is the Heaviside step function. If the function $\phi(x) = \lambda|x|^\alpha$ is introduced in the convolution integral, the resulting NRPD function is:

$$\Phi(x) = \frac{1}{c^{1+\alpha}} \frac{(|x|+K\sigma)^{1+\alpha} - \mathrm{Sg}(|x|-K\sigma)\,||x|-\sigma|^{1+\alpha}}{2K\sigma} \tag{10}$$

where $\mathrm{Sg}(x)$ is the sign function. However, to develop the Eq. (13) we considered only the case $K >> 1$ to use a single convolution integral [26].

The NRPD for the same values of ε, c, a, b is shown in Figure 2-Right. The slope K is close to 11 ($K = 10.5833$). The points represent the numerical data, and the continuous line is the analytical RPD calculated by Eq. (13). There is a good correspondence between the numerical and theoretical data.

Figure 3-Left shows the results for the map (10), considering 150000 reinjected points. Eq. (11) is used to evaluate the RPD, and considering now the approximation $K \approx 0$, resulting:

$$\Phi(x) = \frac{1}{c^{1+\alpha}} \frac{(|x|+\sigma)^{1+\alpha} - \mathrm{Sg}(|x|-\sigma)\,||x|-\sigma|^{1+\alpha}}{2\sigma} \tag{11}$$

Note that Eq. (14) is similar to Eq. (13); in Eq. (14), K is not explicitly present because $K \approx 0$, therefore σ, the noise intensity, governs the reinjection process.

If the slope $K \neq 0$ and K does not reach a high value, it influences the noisy reinjection process, resulting in a more complex RPD structure. Thus, we need to consider the two iteration process until the reinjection to obtain an analytical expression for the NRPD. We consider the map (10) as a composition of the noiseless map (2):

$$x'_n = F(x_n) = -((1+\varepsilon)x_n + x_n^3)e^{(-bx_n^2)} \tag{12}$$

and the map defined as

$$x_{n+1} = R(x'_n) = x'_n + \sigma\xi_n \tag{13}$$

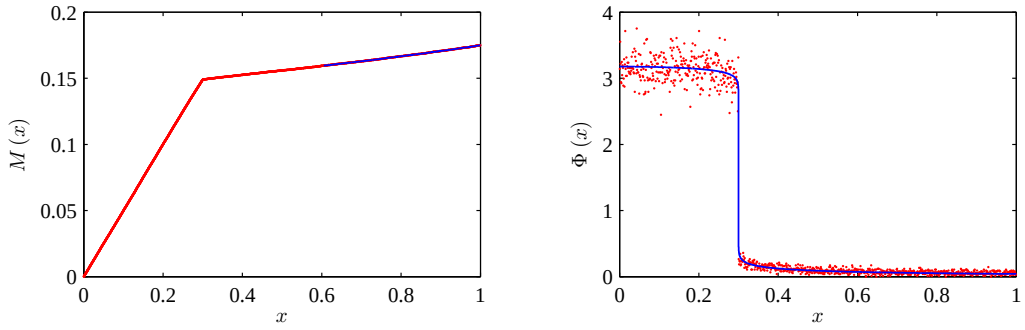

Fig. 3. Map (10). Left: $M(x)$ from the numerical simulations, the darker (blue) line indicates the data used to calculate the exponent α. Right: Theoretical and numerical RPD function, the points correspond to numerical data and the result of Eq. (14) is plotted as a solid line. Parameters: $\varepsilon = 0.005$, $c = 1.0$, $\sigma = 0.3$, $b = 0.05$, $K \cong 0$.

The density function produced by the map (16) can be calculated using the following convolution integral:

$$\rho(x) = \int \rho'(t) G(x-t,\sigma)\,\mathrm{d}t \tag{14}$$

where $\rho'(t)$ is the density produced by the noiseless map given by Eq. (15). If we consider points x_n placed close to the maximum (or minimum) of the map (15), the points x_{n+1} are not directly mapped inside of the laminar interval. It is necessary to consider other iteration to reach the laminar interval:

$$x'_{n+1} = F(x_{n+1}) = -((1+\varepsilon)x_{n+1} + x_{n+1}^3)e^{(-bx_{n+1}^2)} \tag{15}$$

and

$$x_{n+2} = R(x'_{n+1}) = x'_{n+1} + \sigma\xi_{n+1} \tag{16}$$

The resulting density function, applying Eq. (18), can be written as:

$$\rho_l(x) = \frac{dF^{-1}(x)}{dx}\rho(F^{-1}(x)) = K\rho(F^{-1}(x)) \tag{17}$$

Finally, to obtain the noisy reinjection probability density function, $\Phi(x)$, it is necessary to apply a new convolution integral as follow:

$$\Phi(x) = \int \rho_l(y) G(x-y,\sigma)\,\mathrm{d}y \cong \int \rho(y) G(x-y,K\sigma)\,\mathrm{d}y \tag{18}$$

From the previous relations (17) and (21), we note that the amplified noise intensity is given by $(K+1)\sigma$ and the NRPD will have the exponent $\alpha+2$, where α is the exponent for the RPD without noise. Note, that Eqs. (13) and (14) are two extreme cases. For Eq. (13), $K \gg 1$ verifies, we can use the following approximation $(K+1)\sigma \approx K\sigma$. For (14), $K \approx 0$ is verified, therefore, $(K+1)\sigma \approx \sigma$.

The presence of noise not only affects the RPD function, due to the deviations produced on the reinjection trajectories, another reinjection mechanism can arise when the noise strength $(K+1)\sigma$ is relatively large: the adjacent reinjection mechanism (AR). The AR mechanism can be described as follows: when a trajectory has a reinjected point close to the unstable fixed point, the following iterative points increase driven by the parameters of the map until a point, x_j, leaves the laminar interval. If the difference between x_{j+1} (evaluated from maps (1) and (2), without noise) and the laminar boundary c is less or equal than the noise intensity $(x_{n+1} - c \leq (K+1)\sigma)$, the trajectory may return into the laminar interval. The AR concept and its influence in type-II intermittency was recently described in [27].

$$\Phi(x) = \frac{1}{2\sigma(c-x_c)^{(1+\alpha)}} \int [(y+\sigma-x_c)^{(1+\alpha)} - H(y-\sigma-x_c)(y-\sigma-x_c)^{(1+\alpha)}] G(x-y, K\sigma)\, dy \tag{19}$$

5 Noisy RPD without AR and LBR $\neq 0$

In this section we study the LBR influence on the noisy reinjection process without considering the AR mechanism. If no restrictions are imposed to the noise strength ($(K+1)\sigma$) and the LBR (x_s), two different processes can occur. One of them develops when the amplified noise intensity is lower than the LBR, $(K+1)\sigma < x_s$. The other one occurs when the LBR is lower or equal than the amplified noise intensity, $(K+1)\sigma \geq x_s$. Also, for each one of these cases, different expressions for the NRPD will be found, depending on the slope K.

5.1 NRPD without AR and amplified noise intensity $<$ LBR

When $(K+1)\sigma < x_s$, the LBR changes by the noise effect. A "new LBR" arises depending on the original LBR and the amplified noise strength, defined as the difference $x_i = x_s - (K+1)\sigma$. We use the convolution integral (21) to evaluate the NRPD (Φ), explicitly given in Eq. (22). Where $H(x)$ is the Haeviside function, and the expression inside the square brackets is the density, $\rho(x)$, after the first iteration for points close to the local maximum or minimum, x_m (see Eq. (17)). According to the convolution integral the NRPD depends on the value of the slope K, and three cases can appear: $0 < K \leq 1$; $1 \leq K \leq 2$; and $2 \leq K$.

For all the tests that will be considered in this paper we will apply the M methodology to obtain the NRPD. The first step of the M methodoloy is to evaluate the M function from the numerical data. Afterwards we obtain information from $M(x)$; finally we solve Eq. (22) considering different subintervals inside the laminar zone. These subintervals are determined by the overlap of the functions in the convolution integral (22).

5.1.1 NRPD for $0 < K \leq 1$

Figure 4-Left shows $M(x)$ verifying $(K+1)\sigma < x_s$. The used parameters are: $\varepsilon = 0.005$, $b = 0.18$, $x_s = 0.3181$, $K \cong 0.5366$, $c = 1$, $\sigma = 0.2$ and 250000 reinjected points. Then, the new LBR results: $x_i \cong 0.0108$. The function $M(x)$ can be fitted by two straight lines having different slopes that correspond with two regions lying at both side of a small zone around the point $x_c = x_s + (K+1)\sigma \cong 0.6254$. The first one, m_l, is the slope close to the new LBR point (x_i), and m_r is the slope close to the point c (see the darker (blue) line in the figure). Therefore, m_l approximately corresponds to the interval $[x_s - (K+1)\sigma, x_s + (K+1)\sigma)$, and m_r approximately corresponds to $[x_s + (K+1)\sigma, c]$. Similarly to the case without LBR, m_r is very close to the slope of $M(x)$ without noise. The darker (blue) line indicates the points used to calculate $m_r \cong 0.2922$ ($\alpha_r \cong -0.5872$). In the noiseless case $m \cong 0.2913$ and $\alpha \cong -0.5889$. On the other hand, $m_l \simeq 0,685$, on the contrary that was report in [26], here there is not uniform reinjection close to x_i. This occurs because there is not a direct influence of the negative points ($x < 0$) in the evaluation of $M(x)$.

There are two different behaviors between Figures 4-Left and 3-Left. The first one is associated with the matching between the two straight lines. In Figure 4-Left we have small zone, and in Figure 3-Left we obtain only a point x_c. The second difference is due to the m_l value; Figure 4-Left shows that there is not uniform reinjection close to the LBR.

Using Eq. (22), where α is the exponent of the noiseless RPD obtained from $M(x)$ of Figure 4-Left, we get the NRPD given by Eqs. (23), (24), (25) and (26).

To obtain Eq. (23), the interval boundaries are defined by the new LBR and the point $x_s + (K-1)\sigma$; this is the first point where the total overlap between the probability density functions $\rho(x)$ and $G(x)$ occurs. Therefore, in this first interval, these functions only overlap partially. Eq. (24) is obtained solving the convolution integral in the interval $[x_s + (K-1)\sigma; x_s + (1-K)\sigma]$. For points $x \geq x_s + (1-K)\sigma$, $\rho(x)$ changes due to the Heaviside function (see Eq. (22)). Thus to calculate the convolution integral we use here only the first term of $\rho(x)$. Eq. (25) is evaluated inside the third interval, which considers the convolution integral for the points located between $x_s + (1-K)\sigma$ and $x_s + (1+K)\sigma$. Thus, inside this interval the convolution integral is calculated as the sum of two integrals. For one of them we need to consider only the first term of $\rho(x)$ and for the second we require the both terms of $\rho(x)$. To evaluate the convolution integral, for points $x \geq x_s + (1+K)\sigma$, it is necessary to use the both terms in $\rho(x)$. Finally, Eq. (26) is calculated inside the fourth interval, which considers the convolution integral for points located between $x_s + (1+K)\sigma$ and c. Here, the convolution integral is calculated considering the two terms in the expression of $\rho(x)$.

The numerical and theoretical NRPD functions, for the same parameters used in Figure 4-Left, are shown in Figure 4-Right. The points represent the numerical data, and the line represents the analytical NRPD. Note that the analytical results accurately adjust the numerical data.

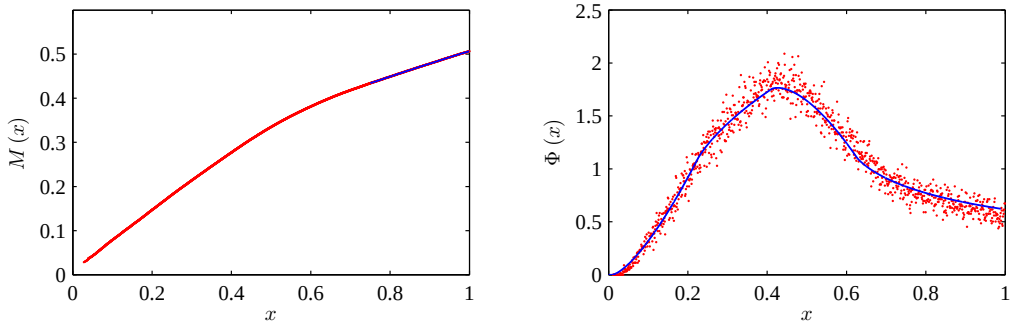

Fig. 4. $(K+1)\sigma < x_s$ and $0 < K \leq 1$. Left: $M(x)$ function, the darker (blue) line shows the data used to calculate the exponent α in Eq.(8). Right: NRPD function, numerical data and theoretical result are represented by points and line respectively. Parameters: $c = 1$, $\varepsilon = 0.005$, $\sigma = 0.2$, $x_s \cong 0.3181$, $K \cong 0.5366$.

For $x_s - (K+1)\sigma \leq x \leq x_s + (K-1)\sigma$

$$\Phi(x) = \Phi_1(x) = \frac{(x+\sigma(1+K)-x_s)^{2+\alpha}}{4(c-x_s)^{(\alpha+1)}\sigma^2 K(\alpha+1)(\alpha+2)} \tag{20}$$

For $x_s + (K-1)\sigma \leq x \leq x_s + (1-K)\sigma$

$$\Phi(x) = \Phi_2(x) = \frac{(x+\sigma(1+K)-x_s)^{2+\alpha} - (x+\sigma(1-K)-x_s)^{2+\alpha}}{4(c-x_s)^{(\alpha+1)}\sigma^2 K(\alpha+1)(\alpha+2)} \tag{21}$$

For $x_s + (1-K)\sigma \leq x \leq x_s + (1+K)\sigma$

$$\Phi(x) = \frac{(x+\sigma(1+K)-x_s)^{2+\alpha} - (x+\sigma(1-K)-x_s)^{2+\alpha} - (x+\sigma(K-1)-x_s)^{2+\alpha}}{4(c-x_s)^{(\alpha+1)}\sigma^2 K(\alpha+1)(\alpha+2)} \tag{22}$$

For $x_s + (1+K)\sigma \leq x$

$$\begin{aligned}\Phi(x) = &\frac{(x+\sigma(1+K)-x_s)^{2+\alpha} - (x+\sigma(1-K)-x_s)^{2+\alpha} - (x+\sigma(K-1)-x_s)^{2+\alpha}}{4(c-x_s)^{(\alpha+1)}\sigma^2 K(\alpha+1)(\alpha+2)} \\ &+ \frac{(x-\sigma(1+k)-x_s)^{2+\alpha}}{4(c-x_s)^{(\alpha+1)}\sigma^2 K(\alpha+1)(\alpha+2)}\end{aligned} \tag{23}$$

Figure 4-Right shows four different behaviors for the NRPD, each one inside of the intervals $[x_s-(K+1)\sigma, x_s+(K-1)\sigma]$, $[x_s+(K-1)\sigma, x_s+(1-K)\sigma]$, $[x_s+(1-K)\sigma, x_s+(1+K)\sigma]$, and $[x_s+(1+K)\sigma, c]$, respectively. This NRPD complex behavior is produced by the iterative process: trajectories starting in points close to local maximum or minimum need, at least, two iterations before the reinjection. Therefore, the noise strongly influences all the reinjection process. Unlike the case with LBR $= 0$, the reinjection is not uniform around the unstable fix point because there is no reinjection from negative x values, thus $x_i > 0$. Three intervals are placed between the new LBR, x_i, and the critical point x_c. Therefore, the combined influence of noise and LBR produces higher effects inside the interval $[x_i, x_c]$. Also, this behavior is shown by the slopes m_l and m_r in Figure 4-Left: m_r is very close to the noiseless $M(x)$ slope, but m_l is not equal to the uniform reinjection case, nor to the noiseless reinjection.

Note that the NRPD given by Eq. (23) - Eq. (26) is represented by a serie of exponential functions with exponent $\alpha+2$, where α is the noiseless exponent. This results is different from that obtained in [26, 30] where the exponent was $\alpha+1$ and the NRPD was more simple. This occurs because the NRPD described in [26, 30] are only particular cases of the NRPD

developed in this work.

5.1.2 NRPD for $1 < K \leq 2$

Some differences appear when $K > 1$, we analyze the interval $1 < K \leq 2$. Figure 5-Left shows $M(x)$ for $\varepsilon = 0.005$, $b = 0.21$, $x_s \cong 0.8076$, $K \cong 1.1750$, $c = 2$, $\sigma = 0.2$ and 150000 reinjected points. Therefore, $(K+1)\sigma < x_s$ is verified. The new LBR results $x_i \cong 0.5901$. $M(x)$ has also two straight lines with slopes m_l and m_r, separated by a reduced zone around the point $x_c = x_s + (K+1)\sigma \cong 1,0251$. The slope m_l corresponds to the interval $[x_s - (K+1)\sigma, x_s + (K+1)\sigma)$, and the slope m_r corresponds to $[x_s + (K+1)\sigma, c]$. m_r is close to the slope of $M(x)$ for the reinjection process without noise. The darker (blue) line indicates the points used to calculate this slope: $m_r \cong 0.32$ ($\alpha_r \cong -0.53$). In the noiseless case $m \cong 0.33$ and $\alpha \cong -0.51$. The behavior of m_l is similar to that described in the previous subsection ($0 < K \leq 1$): $m_l \cong 0.675$.

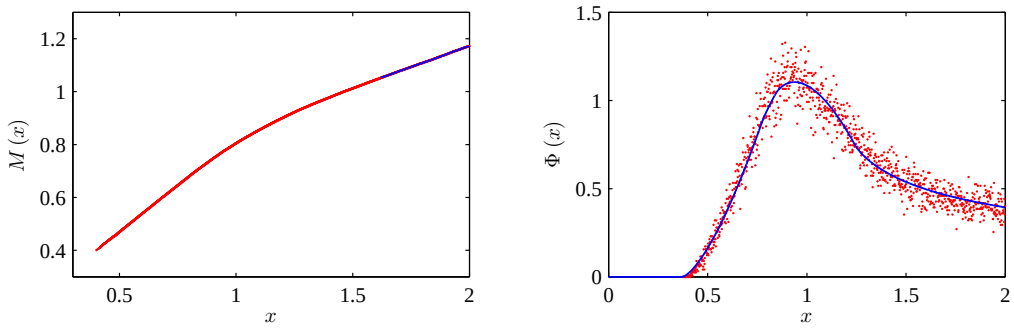

Fig. 5. $(K+1)\sigma < x_s$ and $1 < K \leq 2$. Left: $M(x)$ function, the darker (blue) line shows the data used to calculate the exponent α. Right: NRPD function, the points represent the numerical data and the line is the analytical NRPD. Parameters: $c = 2$, $\varepsilon = 0.005$, $\sigma = 0.2$, $x_s \cong 0.8076$, $K \cong 1.1750$.

To obtain the analytical expression for the NRPD function we solve Eq. (22). We calculate α using m_r from $M(x)$ of Figure 5-Left. The NRPD is given by Eqs. (27), (28), (29) and (30). Figure 5-Right shows the numerical and theoretical NRPD function. To obtain this figure we considered the same parameters used in Figure 5-Left. The points and the line represent the numerical data and the analytical NRPD, respectively. The analytical results verify accurately the numerical data.

The test gives similar results as for the $0 < K \leq 1$ case, but m_r for $0 < K \leq 1$ has a better convergence towards the noiseless slope.

5.1.3 NRPD for $K > 2$

For the case $K > 2$, we calculate the function $\Phi(x)$ using the convolution integral (22). It is given by (31), (32), (33), and (34). As there is no slope $K > 2$ associated with the map (10) we cannot obtain numerical results. Still, the NRPD is similar to those described previously, and is also defined inside four intervals.

5.2 NRPD without AR and amplified noise intensity $\geq$ LBR

We analyze the reinjection behavior when $(K+1)\sigma \geq x_s$ and $\sigma < x_s$. The condition $(K+1)\sigma \geq x_s$ implies that the "new LBR" is $x_i = 0$ and reinjection trajectories coming from points $x < 0$ will occur. The restriction $\sigma < x_s$ implies that the "new LBR" is the origin only when a two iteration reinjection process is considered for trajectories coming from points close to x_m. Then, σ alone is not enough to produce the reinjection from $x < 0$. Also, the function Φ depends on the value of the slope K. Therefore, three cases can appear: $0 < K \leq 1$; $1 \leq K \leq 2$; and $2 \leq K$. To obtain the function Φ we again calculate the convolution integral (22).

Again, we consider the Eq. (10) to evaluate the reinjection process for different slopes K,

5.2.1 NRPD for $0 < K \leq 1$

We study the reinjection process when the following conditions are verified: $(K+1)\sigma \geq x_s$, $\sigma < x_s$, and $0 < K \leq 1$. Following the proposed methodology, the first step is to evaluate $M(x)$. Function $M(x)$ is shown in Figure 6-Left. The parameters are: $b = 0.17$, $\varepsilon = 0.005$, $x_s = 0.194$, $K \cong 0.3459$, $c = 1$, $\sigma = 0.18$ and 150000 reinjected points. Function $M(x)$ shows at least three different behaviors, each one represented by straight lines with different slopes, m_l, m_h and m_r.

For $x_s-(K+1)\sigma \le x \le x_s+(1-K)\sigma$

$$\Phi(x) = \frac{(x+\sigma(1+K)-x_s)^{2+\alpha}}{4(c-x_s)^{(\alpha+1)}\sigma^2 K(\alpha+2)} \tag{24}$$

For $x_s+(1-K)\sigma \le x \le x_s+(K-1)\sigma$

$$\Phi(x) = \frac{(x+\sigma(1+K)-x_s)^{2+\alpha} - (x+\sigma(K-1)-x_s)^{2+\alpha}}{4(c-x_s)^{(\alpha+1)}\sigma^2 K(\alpha+2)} \tag{25}$$

For $x_s+(K-1)\sigma \le x \le x_s+(1+K)\sigma$

$$\Phi(x) = \frac{(x+\sigma(1+K)-x_s)^{2+\alpha} - (x+\sigma(K-1)-x_s)^{2+\alpha} - (x+\sigma(1-K)-x_s)^{2+\alpha}}{4(c-x_s)^{(\alpha+1)}\sigma^2 K(\alpha+2)} \tag{26}$$

For $x_s+(1+K)\sigma \le x$

$$\begin{aligned}\Phi(x) =& \frac{(x+\sigma(1+K)-x_s)^{2+\alpha} - (x+\sigma(1-K)-x_s)^{2+\alpha} - (x+\sigma(K-1)-x_s)^{2+\alpha}}{4(c-x_s)^{(\alpha+1)}\sigma^2 K(\alpha+2)} \\ &+ \frac{(x-\sigma(1+K)-x_s)^{2+\alpha}}{4(c-x_s)^{(\alpha+1)}\sigma^2 K(\alpha+2)}\end{aligned} \tag{27}$$

For $x_s-(K+1)\sigma \le x \le x_s+\sigma$

$$\Phi(x) = \frac{(x+\sigma(1+K)-x_s)^{2+\alpha}}{4(c-x_s)^{(\alpha+1)}\sigma^2 K(\alpha+2)} \tag{28}$$

For $x_s+\sigma \le x \le x_s+(2K-1)\sigma$

$$\Phi(x) = \frac{(x+\sigma(1+K)-x_s)^{2+\alpha} - (x+\sigma(K-1)-x_s)^{2+\alpha}}{4(c-x_s)^{(\alpha+1)}\sigma^2 K(\alpha+2)} \tag{29}$$

For $x_s+(2K-1)\sigma \le x \le x_s+(3K-1)\sigma$

$$\Phi(x) = \frac{(x+\sigma(1+K)-x_s)^{2+\alpha} - (x+\sigma(K-1)-x_s)^{2+\alpha} - (x+\sigma(1-K)-x_s)^{2+\alpha}}{4(c-x_s)^{(\alpha+1)}\sigma^2 K(\alpha+2)} \tag{30}$$

For $x_s+(3K-1)\sigma \le x$

$$\begin{aligned}\Phi(x) =& \frac{(x+\sigma(1+K)-x_s)^{2+\alpha} - (x+\sigma(1-K)-x_s)^{2+\alpha} - (x+\sigma(K-1)-x_s)^{2+\alpha}}{4(c-x_s)^{(\alpha+1)}\sigma^2 K(\alpha+2)} \\ &+ \frac{(x-\sigma(1+K)-x_s)^{2+\alpha}}{4(c-x_s)^{(\alpha+1)}\sigma^2 K(\alpha+2)}\end{aligned} \tag{31}$$

The first line with slope m_l falls inside the interval $[0, |x_s - (K+1)\sigma)|$, where $x_s - (K+1)\sigma \cong 0.05$. The second line with slope m_h falls inside $[x_s - (K+1)\sigma, x_c)$ and the last one, with slope m_r, corresponds to the interval $[x_c, c]$; where $x_c = x_s + (K+1)\sigma \cong 0.4363$. The slope m_l is close to the slope of the uniform reinjection $m_l \cong 0.5135$. The slope m_r is close to the slope of the reinjection process without noise. The darker (blue) line indicates the points used to calculate this slope, and it is $m_r \cong 0.2560$ ($\alpha_r \cong -0.656$). In the noiseless case, we obtain $m \cong 0.2780$ and $\alpha \cong -0.61$. The difference between α_r and the noiseless α is approximately 7%.

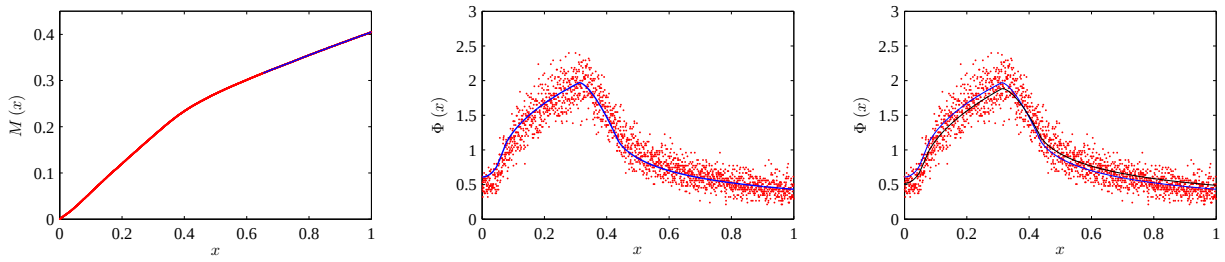

Fig. 6. $(K+1)\sigma \geq x_s$, $\sigma < x_s$ and $0 < K \leq 1$. Left: $M(x)$ function, the darker (blue) line indicates the data used to calculate the exponent α. Center: NRPD function for $\alpha_r = -0.656$. Right: Comparison of the NRPD functions for $\alpha_r = -0.656$ and $\alpha = -0.61$. Parameters: $c = 1$, $\varepsilon = 0.005$, $\sigma = 0.18$, $x_s \cong 0.194$, $K \cong 0.3459$.

Using the convolution integral, Eq. (22), we obtain the analytical expressions for $\Phi(x)$: Eqs. (35), (36), (37), (38) and (39). Here, $\Phi(x)$ is defined in five intervals. The first one had not been considered in the previous sections, and it represents the reinjection for $x < 0$. Note that the straight line with slope m_l appears in the interval with reinjection from $x < 0$.

The numerical data and theoretical NRPD function, for the same parameters used in Figure 6-Left, are shown in Figure 6-Center. To get the theoretical NRPD, we obtain α from $M(x)$ of Figure 6-Left. The numerical results are shown by the points and the line represents the analytical NRPD. A good agreement between numerical and theoretical results is obtained. A better correspondence, principally inside of the interval $[0, x_s + (1-K)\sigma]$, between the theoretical NRPD and the numerical results is obtained for the noiseless exponent α. Figure 6-Right shows the analytical NRPD functions for noisy α_r and noiseless α and the numerical results. The blue (clearer) curve represents the NRPD calculated with $\alpha_r = -0.656$ and the black (darker) one is the NRPD with $\alpha = -0.61$. The last figure shows that the NRPD is sensitive to the exponent α. A good agreement is obtained when the difference between the noisy α_r and the noiseless one is not higher than 10%.

5.2.2 NRPD for $1 < K \leq 2$

The reinjection process satisfying the following conditions: $(K+1)\sigma \geq x_s$, $\sigma < x_s$, and $1 < K \leq 2$ is studied. We evaluate the function $M(x)$ shown in Figure 7-Left. The parameters are: $b = 0.21$, $\varepsilon = 0.005$, $x_s = 0.7961$, $K \cong 1.1669$, $c = 2$, $\sigma = 0.5$ and 250000 reinjected points. The function $M(x)$ is represented by a continuous line. Unlike the previous cases it is not possible to observe two or three straight lines with different slopes. Following the previous sections, we can calculate the exponent α using the points represented by the darker (blue) line resulting $\alpha_r \cong -0.3195$ ($m_r \cong 0.4049$). In the noiseless case, we obtain $\alpha \cong -0.4937$ ($m = 0.3361$). The difference between α_r and the noiseless α is approximately 35,5%. However, the difference between m_r and the noiseless m only is approximately 17%. Also, we calculate a slope $m_l \cong 0.55$ inside the interval $[0, |x_s - (K+1)\sigma)|$, where $|x_s - (K+1)\sigma)| \cong 0.287$. Therefore, very close to the fixed point, the slope m_l is approximately 10% higher than the uniform reinjection slope.

Summarizing, if the noise intensity increases, the exponent α_r obtained, using the noisy $M(x)$, can reduce its accuracy, and, for the last case the analytical results must be evaluated using the noiseless exponent α.

To obtain the NRPD function the convolution integral Eq. (22) is solved. In this test α is the noiseless exponent of the RPD, which is obtained from the noiseless evaluation. The analytical expressions for $\Phi(x)$ are: Eqs. (40), (41), (42), (43) and (44). The numerical and theoretical NRPD functions, for the same parameters used in Figure 7-Left, are shown in Figure 7-Right. The numerical data are represented by points and the line corresponds to the theoretical NRPD. A good correspondence between numerical and theoretical results is observed.

Although, the amplified noise is very high -$(K+1)\sigma > 0.5c$-, the NRPD remains as a sum of exponential functions with exponent $\alpha + 2$; but the noisy $M(x)$ is no longer adequate to correctly calculate the exponent α.

Considering $(K+1)\sigma \geq x_s$ the NRPD is a piecewise function determined by five intervals. Four intervals fall inside $[0, x_s + (K+1)\sigma)$ and the noise strongly affects the zone around to the original LBR, x_s.

For $0 \leq x \leq (K+1)\sigma - x_s$

$$\Phi(x) = \frac{(x+\sigma(1+K)-x_s)^{2+\alpha} - (-x+\sigma(1+K)-x_s)^{2+\alpha}}{4(c-x_s)^{(\alpha+1)}\sigma^2 K(\alpha+1)(\alpha+2)} \tag{32}$$

For $(K+1)\sigma - x_s \leq x \leq x_s + (K-1)\sigma$

$$\Phi(x) = \frac{(x+\sigma(1+K)-x_s)^{2+\alpha}}{4(c-x_s)^{(\alpha+1)}\sigma^2 K(\alpha+1)(\alpha+2)} \tag{33}$$

For $x_s + (K-1)\sigma \leq x \leq x_s + (1-K)\sigma$

$$\Phi(x) = \frac{(x+\sigma(1+K)-x_s)^{2+\alpha} - (x+\sigma(1-K)-x_s)^{2+\alpha}}{4(c-x_s)^{(\alpha+1)}\sigma^2 K(\alpha+1)(\alpha+2)} \tag{34}$$

For $x_s + (1-K)\sigma \leq x \leq x_s + (1+K)\sigma$

$$\Phi(x) = \frac{(x+\sigma(1+K)-x_s)^{2+\alpha} - (x+\sigma(1-K)-x_s)^{2+\alpha} - (x+\sigma(K-1)-x_s)^{2+\alpha}}{4(c-x_s)^{(\alpha+1)}\sigma^2 K(\alpha+1)(\alpha+2)} \tag{35}$$

For $x_s + (1+K)\sigma \leq x$

$$\Phi(x) = \frac{(x+\sigma(1+K)-x_s)^{2+\alpha} - (x+\sigma(1-K)-x_s)^{2+\alpha} - (x+\sigma(K-1)-x_s)^{2+\alpha} + (x-\sigma(1+k)-x_s)^{2+\alpha}}{4(c-x_s)^{(\alpha+1)}\sigma^2 K(\alpha+1)(\alpha+2)} \tag{36}$$

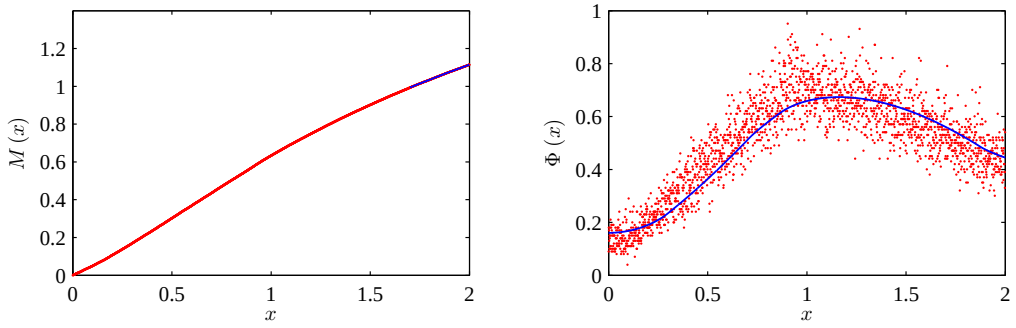

Fig. 7. $(K+1)\sigma \geq x_s$, $\sigma < x_s$, and $0 < K \leq 1$. Left: $M(x)$ function. Right: NRPD function. Parameters: $c = 1$, $\varepsilon = 0.005$, $\sigma = 0.18$, $x_s \cong 0.194$, $K \cong 0.3459$.

6 Effects of adjacent reinjection (AR)

We now analyze the AR effects on maps (9) and (10). When a trajectory reinjects next to the unstable fixed point, the absolute value of the next iterative points increases driven principally by the parameters ε, a and $(K+1)\sigma$, until a point, x_n, leaves the laminar interval. If the difference between $|x_{n+1}|$ (obtained from (1) or (2), without noise) and the laminar boundary $|c|$ is less or equal than the amplified noise intensity ($|x_{n+1}| - |c| \leq (K+1)\sigma$) the trajectory can return into the laminar interval. This behavior is produced by the noise and has been recently defined as adjacent reinjection (AR) [27]. If there is no noise ($\sigma = 0$) there is no AR.

The lower difference $d_l = |x_{n+1} = F(x_n)| - |c|$ is given when $|x_n|$ is replaced by c. For the map (1), using $\varepsilon = 0.01$, $c = 0.4$, $a = 1$, $b = 1.1$, we obtain: $d_l = 0.4662$, implying that the amplified noise should be higher than the semi-length of the laminar interval ($K\sigma > c$) to obtain AR. In that case the noise effects on the RPD are more important than the intermittency

For $0 \leq x \leq (K+1)\sigma - x_s$

$$\Phi(x) = \frac{(x+\sigma(1+K)-x_s)^{2+\alpha} - (-x+\sigma(1+K)-x_s)^{2+\alpha}}{4(c-x_s)^{(\alpha+1)}\sigma^2 K(\alpha+1)(\alpha+2)} \tag{37}$$

For $(K+1)\sigma - x_s \leq x \leq x_s + (1-K)\sigma$

$$\Phi(x) = \frac{(x+\sigma(1+K)-x_s)^{2+\alpha}}{4(c-x_s)^{(\alpha+1)}\sigma^2 K(\alpha+1)(\alpha+2)} \tag{38}$$

For $x_s + (1-K)\sigma \leq x \leq x_s + (K-1)\sigma$

$$\Phi(x) = \frac{(x+\sigma(1+K)-x_s)^{2+\alpha} - (x+\sigma(K-1)-x_s)^{2+\alpha}}{4(c-x_s)^{(\alpha+1)}\sigma^2 K(\alpha+1)(\alpha+2)} \tag{39}$$

For $x_s + (K-1)\sigma \leq x \leq x_s + (1+K)\sigma$

$$\Phi(x) = \frac{(x+\sigma(1+K)-x_s)^{2+\alpha} - (x+\sigma(K-1)-x_s)^{2+\alpha} - (x+\sigma(1+K)-x_s)^{2+\alpha}}{4(c-x_s)^{(\alpha+1)}\sigma^2 K(\alpha+1)(\alpha+2)} \tag{40}$$

For $x_s + (1+K)\sigma \leq x$

$$\Phi(x) = \frac{(x+\sigma(1+K)-x_s)^{2+\alpha} - (x+\sigma(1-K)-x_s)^{2+\alpha} - (x+\sigma(K-1)-x_s)^{2+\alpha} + (x-\sigma(1+k)-x_s)^{2+\alpha}}{4(c-x_s)^{(\alpha+1)}\sigma^2 K(\alpha+1)(\alpha+2)} \tag{41}$$

---

mechanism, and other mathematical techniques are required to analyze the map behavior. A similar behavior is obtained for map (2). If we use $\varepsilon = 0.005$, $c = 1$, $b = 1$, we obtain: $d_l = 1.8142$. The amplified noise $(K+1)\sigma$ should be approximately of the order of c and the noise is stronger than the intermittency phenomenon.

For the type-II intermittency studied in [27], the AR mechanism is important, but in the two maps studied in this work this mechanism is not significant, except for very large amplified noise values where the phenomenon is governed by the noise and the intermittency is hidden.

7 Conclusions

In this work some recent studies proposed in [21, 26, 27, 30] were extended to consider type-III intermittency with nonzero lower boundary of reinjection and high noise intensity. We studied the influence of the noise intensity and the LBR on the reinjection probability density function. Also, the adjacent reinjection mechanism was evaluated.

To carry out this study we implemented a methodology developed recently. It evaluates an auxiliary function, $M(x)$, which is easier to calculate than the RPD. We found that, for LBR $= 0$ the laminar interval can be split in subintervals in which the function $M(x)$ preserves the linear form. However, for LBR $\neq 0$, different behaviors appear. For $(K+1)\sigma <$ LBR a zone where the function $M(x)$ is not linear is displayed. This zone is a matching between two linear behaviors of $M(x)$. For $(K+1)\sigma \geq$ LBR, the function $M(x)$ can be split in three straight lines with different slopes: m_l, m_h and m_r; where m_l corresponds to a uniform reinjection and m_r is approximately equal to the noiseless slope m. Even, for higher noise intensities the function $M(x)$ is represented by a smooth nonlinear curve.

By means of this methodology, it was possible to calculate the noisy RPD function considering the two iteration processes occurring before the reinjection. Thus, it was necessary to solve two convolution integrals. The NRPD is represented by series of exponential functions with exponent $\alpha+2$, where α is the noiseless exponent. The new obtained NRPD presents a more complex structure that those previously published [26, 30]. Also, the exponent $\alpha+2$ is different from that presented before [26, 27, 30].

Through these two iterations occurring before the reinjection, the type-III intermittency trajectories are stretched or

contracted by the derivative $K = dF(x_n)/dx$, where $x_{n+1} = F(x_n)$ is a reinjected point into the laminar zone. The amplified noise generated in the reinjection process can be calculated as $(K+1)\sigma$. The previous studies [26, 30] are only particular cases satisfying $K \approx 0$ or $K \gg 1$.

In all the tests, the numerical data and the theoretical results showed a very good agreement. Note that using the NRPD evaluated from the noisy data, allows to obtain a complete description of the noiseless system, if the noise intensity is not high enough. If the noise strength is high, the noisy $M(x)$ introduces large errors in the evaluation of the noiseless exponent α. We suggest to use the noiseless α to evaluate the NRPD if the difference between the noisy α and the noiseless α is lower than 10%.

The adjacent reinjection was evaluated and its effects on the RPD were analyzed. For the two maps with type-III intermittency studied, the AR mechanism was not important. Only for very high noise intensity values -noise intensities approximately equal to the laminar interval intensity- the AR has influences on the reinjection process. However, for these cases the noise is the principal phenomenon, and the intermittency is hidden by the noise.

Acknowledgements

This research was supported by National University Córdoba, MCyT Córdoba, Polytechnic University Madrid.

References

[1] Manneville, P., and Pomeau, Y., 1979. "Intermittency and lorenz model". *Physic Letter A,* **75**, pp. 1–2.

[2] Manneville, P., 1980. "Intermittency, self-similarity and $1/f$ spectrum in dissipative dynamical systems". *Le Journal de Physique,* **41**, pp. 1235–1243.

[3] Schuster, H., and Just, W., 2005. *Deterministic Chaos*. Wiley VCH, Mörlenbach.

[4] Nayfeh, A., and Balachandran, B., 1995. *Applied Nonlinear Dynamics*. Wiley, New York.

[5] Kaplan, H., 1992. "Return to type-i intermittency". *Physical Review Letter,* **68**, pp. 553–557.

[6] Price, T., and P.Mullin, 1991. "An experimental observation of a new type of intermittency". *Physica D,* **48**, pp. 29–52.

[7] Platt, N., Spiegel, E., and Tresser, C., 1993. "On-off intermittency: A mechanism for bursting". *Physical Review Letter,* **70**, pp. 279–282.

[8] Pikovsky, A., Osipov, G., Rosenblum, M., Zaks, M., and J., K., 1997. "Attractor–repeller collision and eyelet intermittency at the transition to phase synchronization". *Physical Review Letter,* **79**, pp. 47–50.

[9] Lee, K., Kwak, Y., and Lim, T., 1998. "Phase jumps near a phase synchronization transition in systems of two coupled chaotic oscillators". *Physical Review Letter,* **81**, pp. 321–324.

[10] Hramov, A., Koronovskii, A., Kurovskaya, M., and Boccaletti, S., 2006. "Ring intermittency in coupled chaotic oscillators at the boundary of phase synchronization". *Physical Review Letter,* **97**, p. 114101.

[11] Dubois, M., Rubio, M., and Berge, P., 1983. "Experimental evidence of intermittencies associated with a subharmonic bifurcation". *Physical Review Letter,* **16**, pp. 1446–1449.

[12] Stavrinides, S., Miliou, A., Laopoulos, T., and A. Anagnostopoulos, A., 2008. "The intermittency route to chaos of an electronic digital oscillator". *International Journal of Bifurcation and Chaos,* **18**, pp. 1561–1566.

[13] Sanmartin, J., Lopez-Rebollal, O., del Rio, E., and Elaskar, S., 2004. "Hard transition to chaotic dynamics in alfven wave-fronts". *Physics of Plasmas,* **11**, pp. 2026–2035.

[14] Sanchez-Arriaga, G., Sanmartin, J., and Elaskar, S., 2007. "Damping models in the truncated derivative nonlinear schrödinger equation". *Physics of Plasmas,* **14**, p. 082108.

[15] Pizza, G., Frouzakis, G., and Mantzaras, J., 2012. "Chaotic dynamics in premixed hydrogen/air channel flow combustion". *Combustion Theoretical Model,* **16**, pp. 275–299.

[16] Stan, C., Cristescu, C., and Dimitriu, D., 2010. "Analysis of the intermittency behavior in a low-temperature discharge plasma by recurrence plot quantification". *Physics of Plasmas,* **17**, p. 042115.

[17] Chian, A. *Complex System Approach to Economic Dynamics. Lecture Notes in Economics and Mathematical Systems*.

[18] Zebrowski, J., and R., B., 2004. "Type-i intermittency in nonstationary systems: Models and human heart-rate variability". *Physica A,* **336**, pp. 74–86.

[19] Paradisi, P., Allegrini, P., Gemignani, A., Laurino, M., Menicucci, D., and Piarulli, A., 2012. "Scaling and intermittency of brains events as a manifestation of consciousness". In AIP Conference Procceding, Vol. **1510**, AIP, pp. 151–161.

[20] Laugesen, J., Carlsson, N., Mosckilde, E., and Bountis, T., 1997. "Anomalous statistics for type-iii intermittency". *Open System Infarmation Dynamics,* **4**, pp. 393–405.

[21] Elaskar, S., del Rio, E., and Donoso, J., 2011. "Reinjection probability density in type-iii intermittency". *Physica A,* **390**, pp. 2759–2768.

[22] Rosso, O., Larrondo, H., Martin, M., Plastino, A., and Fuentes, M., 2007. "Distinguishing noise from chaos". *Physical Review Letter,* **99**, p. 154102.

[23] Hirsch, E., Huberman, B., and Scalapino, D., 1982. "Theory of intermittency". *Physics Letter A,* **25**, pp. 519–532.

[24] Koronovskii, A., and Hramov, A., 2008. "Type-ii intermittency characteristics in the presence of noise". *European Physics Journal B,* **62**, pp. 447–452.

[25] Kye, W., Rim, S., Kim, C., Lee, J., Ryu, J., Yeom, B., and Park, Y., 2003. "Experimental observation of characteristic relations of type-iii intermittency in the presence of noise in a simple electronic circuit". *Physical Review E,* **68**, p. 036203.

[26] del Rio, E., Sanjuan, M., and Elaskar, S., 2012. "Effect of noise on the reinjection probability density in intermittency". *Communication on Nonlinear Science and Numerical Simulation,* **17**, pp. 3587–3596.

[27] Elaskar, S., del Rio, E., Krause, G., and Costa, A., 2014. "Effect of the lower boundary of reinjection and noise in type-ii intermittency". *Nonlinear Dynamics,* **79**, pp. 1411–1424.

[28] Kye, W., and Kim, C., 2000. "Characteristic relations of type-i intermittency in presence of noise". *Physical Review E,* **62**, pp. 6304–6307.

[29] del Rio, E., and Elaskar, S., 2010. "New characteristic relation in type-ii intermittency". *International Journal of Bifurcation and Chaos,* **20**, pp. 1185–1191.

[30] Elaskar, S., and del Rio, E., 2012. "Intermittency reinjection probability function with and without noise effects". In Latest Trends in Circuits, Automatics Control and Signal Processing, WSEAS, pp. 145–154.

[31] del Rio, E., Elaskar, S., and Makarov, V., 2013. "Theory of intermittency applied to classical pathological cases". *Chaos,* **23**, p. 033112.

[32] del Rio, E., Elaskar, S., and Donoso, J., 2014. "Laminar length and characteristic relation in type-i intermittency". *Communication on Nonlinear Science and Numerical Simulation,* **19**, pp. 967–976.

[33] Krause, G., Elaskar, S., and del Rio, E., 2014. "Type-i intermittency with discontinuous reinjection probability density in a truncation model of the derivative nonlinear schrödinger equation". *Nonlinear Dynamics,* **77**, pp. 455–466.

[34] Krause, G., Elaskar, S., and del Rio, E., 2014. "Noise effect on statistical properties of type-i intermittency". *Physica A,* **402**, pp. 318–329.

[35] del Rio, E., and Elaskar, S., 2016. "The intermittency route to chaos". In Handbook of Applications of Chaos Theory. Christos H. Skiadas, Charilaos Skiadas, Eds. ISBN 9781466590434, CRC Press Book, pp. 3–20.

[36] Elaskar, S., and del Rio, E., 2016. *New advances in chaotic intermittency and applications*. Springer, New York. In press.